Biomedicine & Pharmacotherapy 150 (2022) 113004

Contents lists available at ScienceDirect

Biomedicine & Pharmacotherapy

journal homepage: www.elsevier.com/locate/biopha

A novel PHD2 inhibitor acteoside from *Cistanche tubulosa* induces skeletal muscle mitophagy to improve cancer-related fatigue

Shilei Zhang [a,b], Fukai Gong [c], Jiali Liu [a], Tao Liu [b], Jianhua Yang [a,d,*], Junping Hu [a,**]

[a] Department of Pharmacognosy, School of Pharmacy, Xinjiang Medical University, Urumqi, China
[b] Department of Toxicology, School of Public Health, Xinjiang Medical University, Urumqi, China
[c] Department of Pharmacy, People's Hospital of Xinjiang Uygur Autonomous Region, Urumqi, Xinjiang, China
[d] Department of Pharmacy, Xinjiang Medical University Affiliated First Hospital, Urumqi, Xinjiang, China

ARTICLE INFO

Keywords:
Cancer-related fatigue
Acteoside
Mitophagy
Proline hydroxylase2

ABSTRACT

Objective: To study whether ACT exerts anti-fatigue activity against CRF by inducing skeletal muscle mitophagy via suppressing PHD2 to upregulate the HIF-1α/BNIP3 signaling pathway.
Methods: In this study, the molecular docking virtual screening technique was used to screen active components in *Cistanche tubulosa* that act as potential PHD2 inhibitors; the preliminary verification was carried out by Surface plasmon resonance (SPR) technology. BALB/c mice were treated with Paclitaxel (PTX, 10 mg/kg) and ACT (50, 100 mg/kg) alone or in combination for 20 days. Fatigue-related behaviors, energy metabolism and skeletal muscle mitochondria were assessed. Murine C2C12 myoblast was cultured and differentiated; then, a C26 tumor cell-conditioned medium was added to induce cachexia. Intracellular reactive oxygen species (ROS), mitochondrial membrane potential, mitochondrial microstructure and function, autophagy, PHD2/HIF-1 and PINK1/Parkin signal pathway proteins were analyzed. Then, interfering RNA technology was used to silence PHD2 and observe the efficacy of ACT.
Results: We demonstrated that ACT exerted good binding activity with PHD2; ACT administration ameliorated PTX-induced muscle fatigue-like behavior via improving muscle quality and mitochondria function, increasing mitophagy, upregulating COXIV, CytoC, PINK1, Parkin, HIF-1α and BNIP3 expression and inhibiting p62, LC3B, PHD2 and Beclin-1 expression. The protective effect of ACT disappeared after transfection with the PHD2 gene knockdown plasmid Egln-1-RNAi.
Conclusions: These results suggest that ACT can improve CRF by promoting mitophagy via suppression of PHD2 to remove dysfunctional mitochondria, demonstrating that ACT has huge prospects for clinical application in CRF treatment.

1. Introduction

Cancer-related fatigue (CRF) is the predominant symptom of cancer cachexia and can be observed at any tumor stage [1]. Interestingly, CRF caused by different tumors is often exacerbated after treatment, with an estimated incidence of 25%– 99% during treatment, 65%– 100% after chemotherapy, 82%– 96% after radiotherapy, and 30%– 60% in patients with moderate to severe CRF. Although patients experience relief after effective treatment, follow-up studies found that 25%– 33% of patients experience CRF for several years and can last more than ten years after diagnosis [2]. Unlike general fatigue, CRF cannot be eliminated by rest or sleep. Given the lack of effective treatment measures, the quality of life of cancer patients is seriously affected, thus becoming a major clinical conundrum.

The etiology of CRF is complex, and the pathogenesis remains largely unclear. It has been reported that the tumor itself and the associated

Abbreviations: CRF, cancer-related fatigue; ACT, acteoside; PHD2, proline hydroxylase2; HIF, hypoxia-inducible factor; CPhGs, phenylethanol glycoside from-*Cistanche tubulosa*; PTX, paclitaxel; ROS, reactive oxygen species; SOD, superoxide dismutase; SPR, surface plasmon resonance.

* Corresponding author at: Department of Pharmacognosy, School of Pharmacy, Xinjiang Medical University, Urumqi, China and Department of Pharmacy, Xinjiang Medical University Affiliated First Hospital, Urumqi, Xinjiang, China.
** Corresponding author.
E-mail addresses: zhangsl6191@163.com (S. Zhang), gfkfk@163.com (F. Gong), l2499123234@163.com (J. Liu), xjmult@163.com (T. Liu), h18119185216@163.com (J. Yang), hjp-yft@163.com (J. Hu).

https://doi.org/10.1016/j.biopha.2022.113004
Received 23 March 2022; Received in revised form 14 April 2022; Accepted 17 April 2022
Available online 28 April 2022

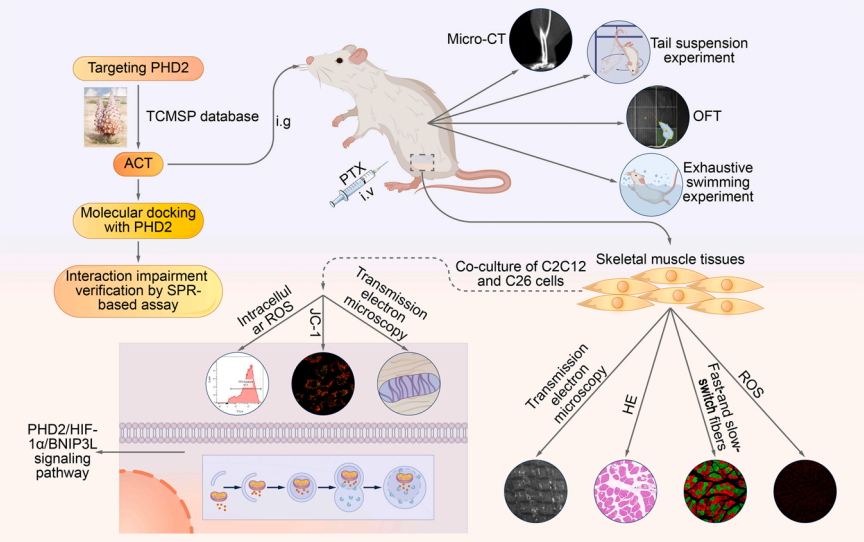

Fig. 1. Workflow scheme. This work was composed of four main parts, including *Cistanche tubulosa* compound selection & SPR verification, in vivo and in vitro experiments.

treatment, complications and sociopsychological factors are the main causes of CRF [3]. Studies have shown that during chemotherapy or radiotherapy, non-target tissues such as skeletal muscle and nerve fibers are affected by the toxicity of chemotherapeutic drugs. In this regard, the structure and function of mitochondria in skeletal muscle have been documented to be destroyed, and the energy supply of muscle cells reduced, leading to an increase of oxidative stress, which causes CRF [4]. In recent years, skeletal muscle mitochondrial dysfunction has become major hot research to improve our understanding of the pathogenesis of CRF [5].

Indeed, studies have shown that mitochondrial dysfunction can also exacerbate hypoxia in tumor environments. The predominant subjective feeling in patients with tumor-associated anemia is fatigue [6]. Anemia is common in CRF patients, which leads to inhibited mitochondrial function and aggravates hypoxia in tumor patients [7]. Accordingly, maintaining mitochondrial homeostasis and timely removal of damaged mitochondria in skeletal muscle under long-term hypoxic stress conditions seems to be an effective intervention strategy to alleviate CRF in cancer patients [8].

It has been established that mitophagy plays a crucial role in clearing dysfunctional mitochondria, fine-tuning the number of mitochondria and maintaining energy metabolism [9,10]. Hypoxia-inducible factor (HIF) has been shown to be an important regulator of cellular oxygen homeostasis, while Proline hydroxylase2 (PHD2) is a key enzyme that regulates the stability of HIF-1α [11]. Under hypoxic conditions, the activity of PHD2 is inhibited, which prevents the hydroxylation and degradation of HIF-1α. HIF-1α accumulates, translocates into the nucleus, binds to HIF-1β to form a heterodimer that acts as a transcription factor and induces mitophagy by regulating the expression of BNIP3/Beclin-1 [12]. A series of recent studies have substantiated that many drugs can treat CRF caused by anemia by improving the function of HIF via inhibition of PHD [13,14].

At present, there is no FDA-approved drug that can effectively prevent and treat CRF. An increasing body of evidence suggests that natural products of various sources have a lot of pharmacological effects and are expected to become new alternative drugs for managing CRF [15]. *Cistanche tubulosa* (family Orobanchaceae) is a parasitic plant widely grown in the southern region of Xinjiang in China. *Cistanche tubulosa* has been shown to exhibit various properties, including enhancing organism immunity, improving organism endurance, nourishing the kidneys, treating impotence, anti-oxidation and anti-aging [16]. This plant contains phenylethanol glycoside (CPhGs), iridoid and polysaccharides, of which the echinacoside and ACT are the main bioactive species.

In a previous study, we found that the HIF-1 pathway ranked second among the top 20 related pathways as common targets of *Cistanche tubulosa* and CRF by the network pharmacology. In the present study, we used molecular docking technology to search for potential active components similar to PHD2 inhibitors in *Cistanche tubulosa* and SPR to verify their binding activity. The results showed that ACT ranked first among all compounds with a docking score of − 11.184 and KD (M) value of 11.6 μM, suggesting that ACT has a good binding activity with PHD2 protein. However, the association between ACT and skeletal muscle mitophagy remains unclear and warrants further exploration.

In this study, the effects of ACT on PTX-induced fatigue in mice were investigated by performing a series of behavioral tests, analyzing the quality of skeletal muscle and the state and function of mitochondria, etc. Furthermore, a malignant cachexia model of muscle cells induced by co-culture of C26 and C2C12 cells was established to investigate the mitophagy of ACT and the effect of mitophagy signaling pathways PHD2/HIF-1α/BNIP3 and PINK1/Parkin (See workflow scheme in Fig. 1). Our experimental results showed that ACT alleviated CRF by promoting mitophagy via suppressing PHD2 to remove dysfunctional mitochondria, which indicates that ACT has huge prospects as a novel drug for CRF treatment.

2. Materials and methods

2.1. Reagents and antibodies

C2C12 (CL-0044) and C26 cells line (CL-0071) were purchased from Procell Life Science&Technology Co.,Ltd. (Wuhan, China). ACT (HPLC>98.5%) was obtained from Yongjian Pharmaceutical Co., Ltd (Taizhou, China). PTX Injection was purchased from Yangtze River Pharmaceutical Group (Taizhou, China). The Mitochondrial membrane potential assay kit with JC-1 and total superoxide dismutase assay kit with WST-8 were obtained from Beyotime (Shanghai, China). The Reactive oxygen species assay kit was purchased from Solarbio Science & Technology Co., Ltd. (Beijing, China). The following primary antibodies were used in this study at the indicated dilution for western blot (WB) and immunofluorescence (IF) analysis: COXⅣ (GB11250, Servicebio, 1:1000 for WB), CytoC (GB11080, Servicebio, 1:1000 for WB), p62 (GB11239–1, Servicebio, 1:1000 for WB), LC3B (18725–1-AP, Proteintech, 1:500 for WB), PHD2/Egln1 (19886–1-AP, Proteintech, 1:700 for WB), HIF-1α (GB111339, Servicebio, 1:700 for WB), BNIP3L

(12986–1-AP, Proteintech, 1:700 for WB), Beclin-1 (GB112053, Servicebio, 1:700 for WB), PINK1(23274–1-AP, Proteintech, 1:600 for WB), Parkin(GB113802, Servicebio, 1:700 for WB), Fast Myosin Skeletal Heavy chain (GB112130, Servicebio, 1:700 for IF), Slow Myosin Skeletal Heavy chain (GB111857, Servicebio, 1:300 for IF), and β-actin (GB11001, Servicebio, 1:1000 for WB). The Peroxidase-conjugated second antibody was purchased from Proteintech (SA00001–2, Wuhan, China).

2.2. Screening of active compounds in Cistanche tubulosa targeting PHD2

2.2.1. Selection of the screening database

To screen for potential compounds of *Cistanche tubulosa* that target PHD2, we downloaded the chemical structure of compounds in *Cistanche tubulosa* from the TCMSP database. ISIS software was used to intersect and merge the compounds. Finally, we established the database of traditional Chinese medicine in *Cistanche tubulosa*. At the same time, the binding data of PHD2 inhibitors were retrieved in the BindingDB website, using the keyword "PHD2" and processed by 1) Deleting the activity data of repetitive structures. 2) Removing the activity data value of the wrong structure based on the original literature. 3) Selecting a threshold of the activity data value of 10000 nM. 4) Removing compounds with complex molecular formulas. After meeting these four conditions, non-repetitive PHD2 inhibitors were selected, and a database of PHD2 inhibitors was established by ISIS software.

2.2.2. Molecular docking analysis

The flexible docking process between chemical compounds and target proteins was conducted by the Rosetta software. A total of 30 docking conformations were extracted and ranked according to the docking energy value. The detailed docking process was performed as follows: 1) A wide range of boxes was formed using the amino acid residues around the receptor's active site. Different atoms were used as probes to scan and calculate the lattice energy. 2) A conformational search was carried out on the ligands within the box range. Finally, the ligands were scored according to their different conformations, orientation, position and energy, and the results were sorted. 3) For 501 traditional Chinese medicine component systems, protein-small molecule semi-flexible docking was carried out, yielding 100 docking phases, ranked by the energy levels. The molecules with the most clustering and the lowest energy were selected as the representatives of each system.

2.3. Surface plasmon resonance (SPR) assay

SPR analysis was conducted with the Open SPR instrument (Nicoyalife, Canada). The NTA sensor chip was first installed on the OpenSPR instrument in accordance with the standard operating procedure. In the beginning, a maximum flow rate of 150 μm L/min was used, and the detection buffer consisted of 1%DMSO + PBS (pH 7.4). After reaching the signal baseline, the flow rate of the buffer was adjusted to 20 μL/min. After activating the chip, the prepared nicl2 solution was injected through the injection port and functionalization of the chip surface was completed. Then, 200 μL of the dissolved ligand protein was prepared and injected through the injection port over 4 min. The baseline was observed for 5 min to ensure stability. The ligand-binding affinity was measured by comparing the signals before and after ligand injection. More ligands could be injected if needed. After the ligand signal was stable, a high concentration of analyte was injected to confirm the activity of the ligand and the approximate maximum binding capacity of the surface. The flow rate was increased to 150 μL/min, and the appropriate regeneration buffer was injected to remove analytes. The analyte was diluted with buffer, and the concentration of the analyte was detailed in the experimental results. The binding time between protein and ligand was 240 s, and the natural dissociation was 360 s by injection of the running buffer at a flow rate of 20 L/min. The data were analyzed with TraceDrawer (Ridgeview Instruments ab, Sweden) using a standard one-to-one binding model.

2.4. In vivo experiments

2.4.1. Animal models and drug treatment

BALB/c (males; weighing 16–20 g) mice were purchased from the Animal Experiment Center of Xinjiang Medical University; the animal certificate number and SPF environment use license number were SCXK (Xin) 2018–0001 and SYXK (Xin) 2018–0003. Before the experiment, all mice were adaptively fed in a specific pathogen-free (SPF) environment for 7 days at a room temperature of 22–26 ℃, relative humidity of 40–60%, under a 12/12 h light/dark cycle for 12 h, with free access to food and water.

Before administration, male BALB/c mice were placed in a swimming box (high 30 cm, diameter 25 cm) for adaptive swimming training for 7 days; the water temperature was 25 ℃ ± 1 ℃. According to the swimming time, the mice were randomly divided into 4 groups (n = 24): normal control (NC) group, PTX group, PTX + 50 mg/kg ACT group, and PTX + 100 mg/kg ACT group. 50 mg/kg and 100 mg/kg ACT were administered intragastrically once daily. 10 mg/kg PTX was administered by intraperitoneal injection, once every 2 days. After the animals were separated into different groups, the drugs were administered for 21 days. The normal control group was administered with the corresponding volume of normal saline intragastrically.

2.4.2. Ethology assessment

To reflect the degree of fatigue of each group of mice, the exhaustive swimming test, open field test and tail suspension test were used.

Exhaustive swimming test: Prior to administration and on days 10 and 20 after administration, lead pendants (weighing 7% of the bodyweight) were attached to the tail of mice. The mice in each group were put into a swimming box with a water temperature of 25 ℃ ± 1 ℃ (high 30 cm, diameter 25 cm), and the exhaustive swimming time was recorded. Exhaustive swimming was observed when the tip of the mouse nose sank under the water for at least 10 s

The open-field test was carried out using Chengdu Tai League TM-visual behavior experiment system. Mice were put into the center of the box, and the total distance moved and immobility time were observed for 5 min. Each mouse was tested after thorough cleaning of the box.

Tail suspension test: all mice in the open-field experiment were treated according to the original grouping and administration plan. 30 min after the last administration, the mouse tail (from the tail tip 2 cm) was glued to the TS-200 tail suspension tester, the mouse head was placed 5 cm from the bottom of the tester, and the immobility time was recorded for 5 min

2.4.3. Micro-CT

To evaluate the changes in skeletal muscle content in each group of mice, the mice underwent Micro-CT (SkyScan 1176, Bruker, Germany). Before the analysis, the mice were anesthetized with a 3% isoflurane/oxygen mixture and placed prone on the Micro-CT bed, keeping the hind limbs in a natural position for scanning. The following parameters: the distance from the upper end of the tibia to the medial malleolus (tibia length, L), and the vertical distance from the half-length of the tibia to the outer edge of the hindlimb muscle (muscle thickness, T), were measured. The Muscle mass index (IMM) was defined as the ratio of T to L, and the cross-sectional area of tibial muscles at half-length was measured by the ROI contour tool in Micro View analysis software. The left and right legs of each mouse were analyzed, and the average value was taken.

2.4.4. Histological, Immunofluorescence staining and Reactive oxygen species measurements

At the end of the experiment, the skeletal muscle tissues were fixed in 10% Neutral Buffered Formalin for histological analysis under light

microscopy. 3–5 mm-thick skeletal muscle tissue sections were deparaffinized and processed routinely for hematoxylin and eosin (H&E) and immunofluorescence staining of the fast- and slow-twitch fibers. The frozen skeletal muscle tissues were taken out from a − 80 °C refrigerator and immediately embedded in the OCT compound. The OTC samples were cut into 10 μm-thick sections, incubated in DHE, and mounted with DAPI. Once DHE was oxidized to ethidium and subsequently intercalated to DNA, a bright red fluorescence was observed. Images were obtained using the fluorescence microscope (DMi8, Leica, Germany) and analyzed with Image lab software.

2.4.5. Detection of superoxide dismutase

Total superoxide dismutase (SOD) activity was measured using the total superoxide dismutase assay kit with WST-8(S0101M, Beyotime, China). Skeletal muscle tissues were weighed and homogenized with SOD sample preparation solution on ice. Lysis samples were centrifuged at 1000 g for 10 min at 4 ℃. Twenty microliters of the diluted samples were added to 160 μL of the WST-8 working solution, then 20 μL of the initial solution was added. The SOD activity was analyzed at 450 nm after 30 min incubation at 37 ℃. Meanwhile, the absorbance of blank 1 (buffer + WST-8 working solution + start solution) and blank 2 (buffer + WST-8 working solution) was determined and used to calculate sample results according to the manufacturer's instructions. The results of SOD activity were expressed as U/g protein.

2.4.6. Transmission electron microscope of skeletal muscle

The skeletal muscle tissues were post-fixed in 1% osmium tetroxide for 3 h. After dehydration with graded ethanol and acetone, samples were embedded in Spurr, sliced into pieces with the thickness of 70 nm, stained with uranyl acetate and lead citrate, and observed using TEM (JEM1230HC, JEOL, Japan). The mitochondrial Flameng score was evaluated at 10,000 × .

2.5. In vitro experiments

2.5.1. Cell culture

C2C12 cells were cultured in a high glucose DMEM medium supplemented with 10% fetal bovine serum(FBS, Gibco, Australia) and the high glucose DMEM differentiation medium supplemented with 2% Horse serum(HS, Procell, China). C26 cells were cultured in a high glucose DMEM medium supplemented with 10% FBS and 1% penicillin and streptomycin. All cells were cultured at 37 ℃ with 5% CO2.

2.5.2. Drug administration

ACT was diluted with the cell culture media before use. C2C12 cells were divided into the Control group, C26 co-culture model group and C26 co-culture model + ACT group. The control group consisted of well-differentiated cells in normal culture media. In the C26 co-culture model group with C2C12 cells, C26 cells were cultured in high glucose DMEM medium containing 2% HS for 24 h; the culture medium was collected into a centrifuge tube and underwent centrifugation at 1000 r/min for 5 min. The upper liquid was absorbed without contact with the bottom sediment, and a 100% conditioned medium was prepared. The 100% C26 medium was diluted to a 33% conditioned medium and co-cultured with differentiated C2C12 cells. In the C26 co-culture model + ACT group, cells were treated with different concentrations of ACT (25, 50 and 100 μM) and 33% conditioned medium for 24 h.

2.5.3. Cell counting Kit-8 assay

CCK-8 assay (BA00208, Bioss, China) was conducted to determine the viability of C2C12 cells, according to the manufacturer's instructions. Cells exhibiting logarithmic growth were seeded in a 96-well plate at a density of 5 × 103 cells/ well. After incubation for 24 h and 48 h, 20 μL CCK-8 reagent was added to each well. A microplate reader (ThermoFisher, USA) at 450 nm was applied to detect the viability of cells. Samples were run for each concentration in quadruplicates. The following formula (Eq. (1)) was used to calculate the percentage of cell viability:

$$\text{Cell viability (\%)} = (\text{mean absorbency in test wells - mean absorbency in blank wells})/(\text{mean absorbency in control wells - mean absorbency in blank wells}) \times 100 \quad (1)$$

2.5.4. Detection of ROS by flow cytometry

Generation of intracellular ROS was measured using 2,7′-dichlorofluorescein-diacetate (DCFH-DA, CA1410, Solarbio, China). C2C12 cells were cultured in a high glucose DMEM differentiation medium supplemented with 2% HS, 1% penicillin and streptomycin, at 37 ℃ in 5% CO2, and treated with 33% C26 conditioned medium and different concentrations of ACT for 24 h, then incubated with DCFH-DA (10 μM) for 30 min at 37 ℃. After being washed twice with serum-free culture media, the level of ROS was determined using a flow cytometer (Becton Dickinson, San Jose, US). DCFH-DA positive cells with high ROS levels were analyzed using FlowJo software (version 10, FlowJo LLC).

2.5.5. Mitochondrial membrane potential measurement

The mitochondrial membrane potential was measured using a JC-1 fluorescent probe (C2006, Beyotime, China). The C2C12 cells were cultured in a high glucose DMEM differentiation medium supplemented with 2% HS, 1% penicillin and streptomycin, at 37 ℃ in 5% CO2, treated with 33% C26 conditioned medium and different concentrations of ACT for 24 h and then incubated with JC-1 for 20 min at 37 ℃. The stained cells were washed twice and analyzed using a confocal laser scanning microscope (C2, Nikon, Japan). Mitochondrial depolarization was indicated by a decrease in red/green fluorescence intensity ratio.

2.5.6. Transmission electron microscope of C2C12 cells

C2C12 cells were fixed with 2.5% glutaraldehyde and then post-fixed with 1% osmium tetraoxide, dehydrated in a graded series of ethanol concentrations and embedded in epoxy resin. The ultrathin sections were mounted on copper grids and then double-stained with uranyl acetate and lead citrate. The samples were examined and photographed under a JEOL electron microscope (JEM1230 HC, JEOL, Japan). The number of autolysosomes and mitochondrial Flameng score were evaluated at 40,000 × .

2.5.7. Western blotting assay

Total proteins of cells were isolated by radioimmunoprecipitation assay (RIPA) lysis buffer (89901, ThermoFisher, USA) and quantified using a BCA detecting kit (G2026, Servicebio, China). Proteins were separated by SDS-poly-acrylamide gel electrophoresis and transferred to PVDF membranes. Membranes were blocked with 5% fat-free milk in TBST buffer at room temperature for 2 h and then incubated overnight with rabbit anti-LC3B, p62, COXⅣ, CytoC, PHD2, HIF-1α, BNIP-3, beclin-1, PINK1 and Parkin at 4 ℃. The membranes were washed three times in TBST and incubated with goat anti-rabbit conjugated secondary antibody (1:25 000 dilution) for 1 h at room temperature. Finally, the film was exposed, developed and fixed to observe the results. The gray value of each special band on the image was digitized by ImageJ software V1.8 (National Institute of Health), with β-actin serving as the internal reference.

2.5.8. Plasmid DNA, siRNA, and transfection

The C2C12 cells were maintained in a high glucose DMEM differentiation medium supplemented with 2% HS, 1% penicillin and streptomycin, at 37 ℃ in 5% CO2 and treated with a 33% C26 conditioned medium. Then, C2C12 cells were transfected with a plasmid expressing the constitutively active form of PHD2 and vector control (GeneChem, Shanghai, China) using Lipofectamine 3000 (Invitrogen, Carlsbad, CA) according to the manufacturer's instructions. Briefly, cells in the 6-well

Table 1
TCMSP database (components of *Cistanche tubulosa*) molecular system binding model (sorted by energy score, all compound molecules ranked in the top 10).

Title	chemical compound	docking score	XP GScore	glide gscore
MOL003333	acteoside	-11.184	-11.203	-11.203
MOL003202	8-epi-Loganic acid	-10.718	-10.718	-10.718
MOL008872	cistanoside B	-10.419	-10.419	-10.419
MOL000346	succinic acid	-10.415	-10.421	-10.421
MOL008876	echinacoside_qt	-9.271	-9.271	-9.271
MOL005320	arachidonate	-9.164	-9.167	-9.167
MOL008861	Cistanoside F	-8.471	-8.472	-8.472
MOL001669	geniposidie acid_qt	-8.205	-8.22	-8.22
MOL008859	Cistanoside E	-8.111	-8.111	-8.111
MOL008857	Cistanoside A	-7.92	-7.92	-7.92

plates were incubated with plasmid /Lipofectamine 3000 complex at 37 ℃ for 48 h, and the medium was replaced with the concentration of ACT 50 μM for 24 h. Then, the cell lysates were collected for ROS content and verified by Western blot.

2.6. Statistical analysis

SPSS 20.0 was used for statistical analyses. The measurement data were expressed as mean ± standard deviation (SD). One-way ANOVA was performed for multiple group comparisons and the LSD test for the difference between two groups. A P-value < 0.05 was statistically significant.

3. Results

3.1. ACT was selected as a key compound with anti-PHD2 potential

To screen for potential compounds of *Cistanche tubulosa* that target PHD2, the Traditional Chinese Medicine Systems Pharmacology Database and Analysis Platform (TCMSP) was retrieved. Next, the topological parameters of each selected compound, including the conformation, orientation, position and energy, were calculated and scored using protein-small molecule semi-flexible docking. The molecules with the most clustering and the lowest energy were selected as the representatives of each system. The top 9 compounds with scores from high to low are shown in Table 1 and Fig. 2C (the rest of the compounds are listed in Supplementary Table 1). Among these, ACT (PubChem CID: 5281800) exhibited the highest potential binding activity with PHD2 (Fig. 2D). Accordingly, ACT was selected as a key compound for further analysis. The molecular formulas and chemical structures of ACT are shown in Fig. 2A.

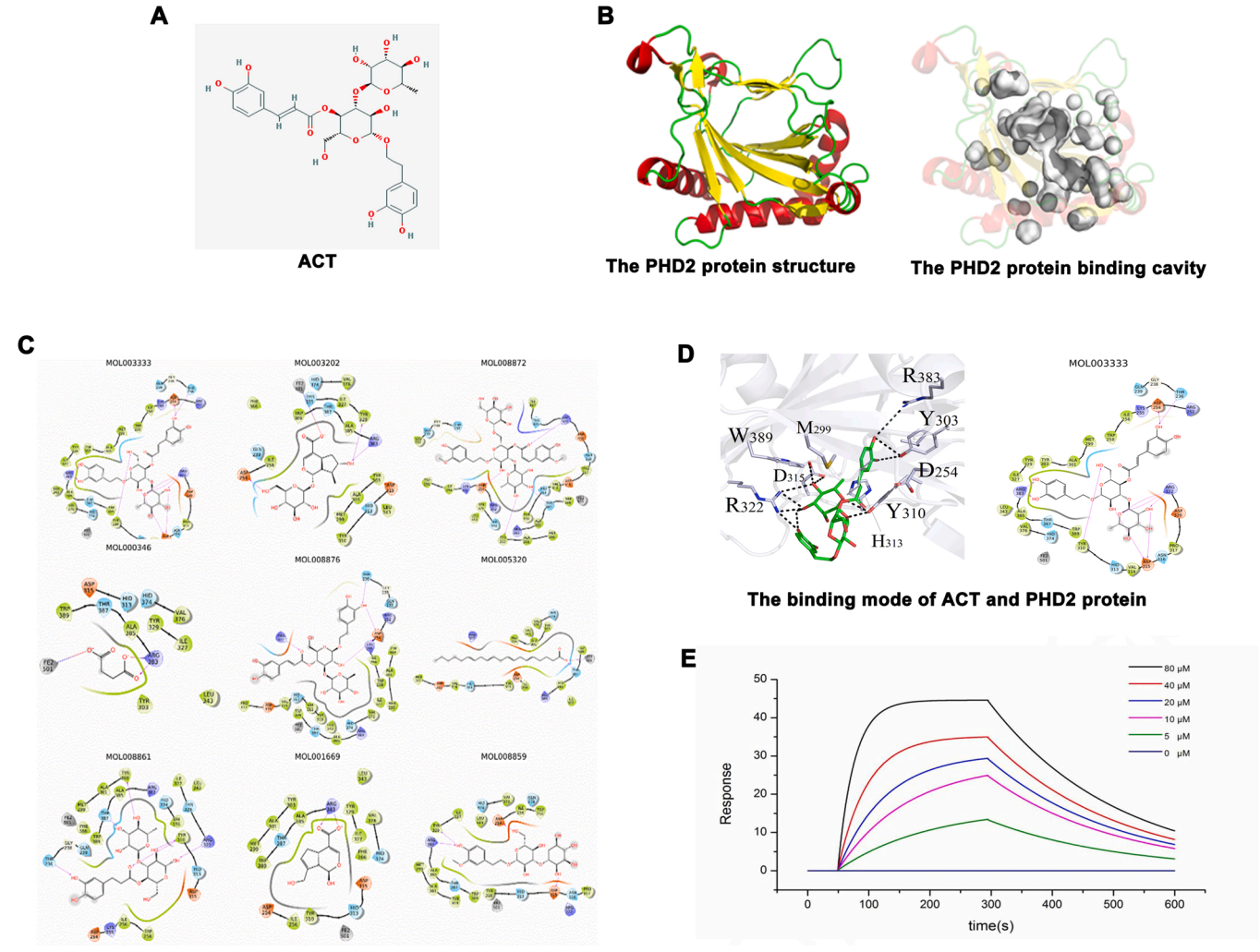

Fig. 2. Selection of the key compounds from *Cistanche tubulosa*. A, the 2D-chemical structure of ACT downloaded from the TCMSP database; B, PHD2 protein structure and molecular docking cavity; C, TCMSP database (components of *Cistanche tubulosa*) molecular system binding model (sorted by energy score, all compound molecules ranked in the top 9); D, the binding pattern of ACT to PHD2 protein; E, interactions between the ACT and PHD2 were determined by SPR assay, The KD of the PHD2 protein with a series of concentrations of ACT was calculated by SPR.

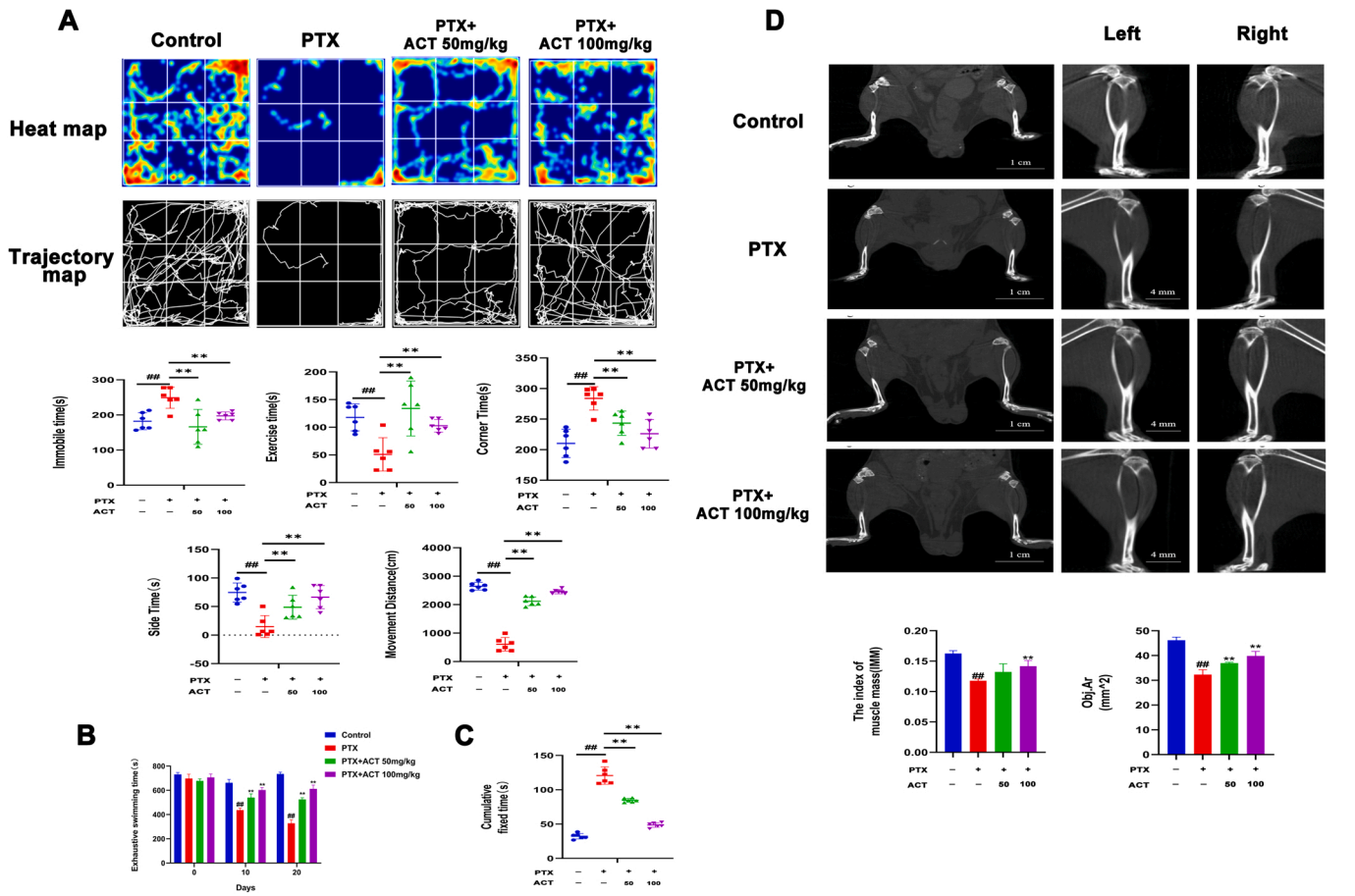

Fig. 3. Alleviating effect of ACT on PTX-induced cancer-related fatigue. 50 mg/kg and 100 mg/kg ACT were administered intragastrically, once daily. 10 mg/kg PTX was administered by intraperitoneal injection, once every 2 days. A, the results of the open field test in each group of mice; B, the degree of fatigue was evaluated by the exhaustive swimming time test; C, the results of tail suspension test in each group of mice (Mice struggled to escape for a period of time and adopted a posture of immobility. The cumulative immobility time of the animal was recorded during the course of the experiment); D, micro-computed tomography for non-invasive evaluation of muscle mass in mouse models of cancer-related fatigue induced by PTX. The values are presented as mean ± SD. #P < 0.05, ##P < 0.01, compared with control group, *P < 0.05, **P < 0.01, compared with model group.

3.2. Interactions between ACT and PHD2 were validated by the SPR assay

The interactions between ACT and PHD2 were further evaluated by real-time biomolecular interaction analysis and SPR. The kinetics of the binding reaction were determined by injecting different concentrations of the compounds over a recombinant human PHD2 (Egln1) immobilized on the chip surface. The data were fitted to a monovalent binding model by non-linear regression. The equilibrium dissociation constants (KD) for ACT and PHD2 were 1.16e-5, respectively, with association rates of 4.09e2 and dissociation rates of 4.75e-3 (Fig. 2E).

3.3. Effect of ACT on exhaustive swimming time

The exhaustive swimming test, open field test and tail-suspension experiment were used to evaluate the anti-fatigue properties of ACT. The results showed no significant difference in exhaustive swimming time among each group ($p > 0.05$) at baseline. The exhaustive swimming time of mice in the ACT (50, 100 mg/kg)-treated groups was significantly higher than in the PTX group on days 10 and 20 ($p < 0.01$) (Fig. 3B).

3.4. Effect of ACT on the open field test

The open field test results in each group of mice can be observed in Fig. 3A. The results showed that ACT (50, 100 mg/kg) significantly reduced the immobility times and corner zone times of mice compared to the PTX group ($p < 0.01$). Moreover, ACT (50, 100 mg/kg) also improved the exercise time, the total exercise distance and center time compared to the PTX group ($p < 0.01$).

3.5. Effect of ACT on the tail suspension experiment

As shown in Fig. 3C, the cumulative resting time of the PTX group was significantly longer than the control group. Compared with the PTX group, the cumulative resting time of the PTX + 50 mg/kg ACT group and the PTX + 100 mg/kg ACT group were significantly shorter ($p < 0.01$). These findings suggest that ACT exerts potent anti-fatigue effects.

3.6. Micro-CT changes of the Effect of ACT on skeletal muscle content

We previously established that mice in the PTX group had poor endurance and were more prone to fatigue. Given the key role of skeletal muscle loss in CRF, we sought to assess the skeletal muscle content of these mice; a well-established imaging macroscopic evaluation method was used to evaluate the skeletal muscle content of mice in each group. As seen in Fig. 3D, the muscle mass index of the PTX group was lower than the control group($p < 0.01$), while 100 mg/kg ACT could significantly accentuate the decrease of muscle mass index induced by PTX ($p < 0.01$). Similar results were also obtained on the index of the cross-sectional area of muscle groups in half-length($p < 0.01$).

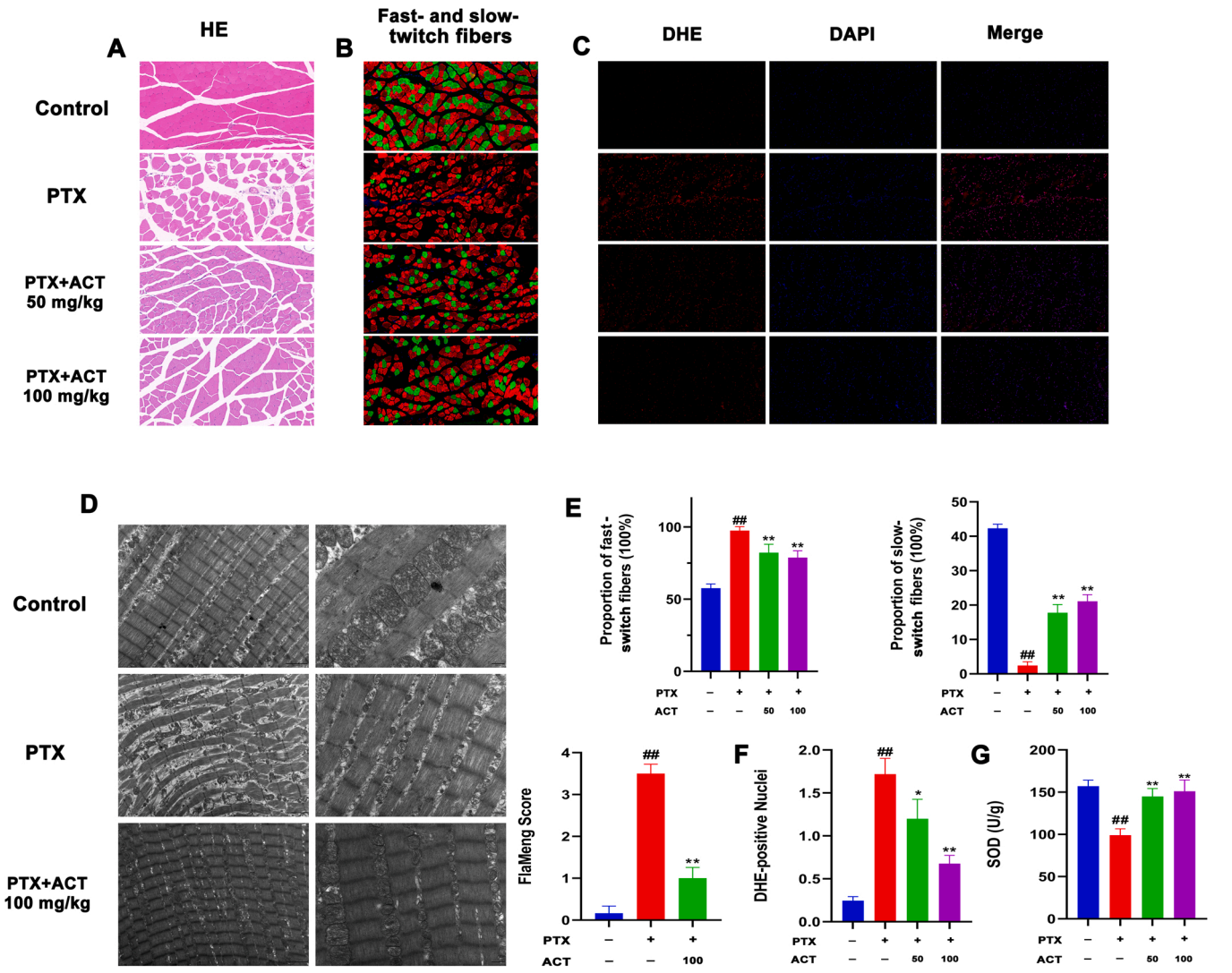

Fig. 4. Mechanism of ACT treatment in improving cancer-induced fatigue in mice. 50 mg/kg and 100 mg/kg ACT were administered intragastrically, once daily. 10 mg/kg PTX was administered by intraperitoneal injection, once every 2 days. A, Photomicrographs of skeletal muscle sections stained with H&E (200X); B and E, immunofluorescence staining of fast and slow-twitch muscle fibers (red represents fast muscle fibers, green represents slow muscle fibers, 200X); C and F, ROS fluorescence staining(100X), DHE can enter the cell freely through living cells and be oxidized by intracellular ROS to form oxidized ethidium. Oxidized ethidium can be incorporated into chromosome DNA to produce red fluorescence. The amount and change in ROS content were assessed according to the red fluorescence in frozen sections of skeletal muscle tissue; D, representative images of the mitochondrial ultrastructure in skeletal muscle sections under transmission electron microscopy (scale bar =2 μm and 500 nm). G, SOD content in skeletal muscle tissues. The values are expressed as mean ± SD of three independent experiments. #P < 0.05, ##P < 0.01, compared with control group, *P < 0.05, **P < 0.01, compared with model group. (For interpretation of the references to color in this figure legend, the reader is referred to the web version of this article.)

3.7. Histopathology changes of the effect of ACT on skeletal muscle

HE staining results showed that the cross-sectional muscle area in the PTX group was significantly smaller than in the control group, suggestive of significant skeletal muscle atrophy. Consistently, 50 mg/kg ACT and 100 mg/kg ACT could significantly improve skeletal muscle atrophy in mice (Fig. 4A).

3.8. Effects of ACT on fast and slow muscle fibers of skeletal muscle

It is widely acknowledged that skeletal muscles have differences in the contraction speed and anti-fatigue ability and are generally divided into fast-twitch muscle fibers (type II muscle fiber mainly) and slow-twitch muscle fibers (type I muscle fiber mainly) based on the difference in tissue structure, and the distribution and composition of muscle fibers. The results of fast and slow-twitch muscle fibers staining (Fig. 4B, E) showed that compared with the control group, the proportion of fast-twitch muscle fibers in the PTX group increased significantly ($p < 0.01$), while the proportion of slow-twitch muscle fibers decreased significantly in PTX group ($p < 0.01$). Compared with the PTX group, the proportion of fast-twitch muscle fibers was significantly reduced, and the proportion of slow-twitch muscle fibers increased in the PTX + 50 mg/kg ACT group and PTX + 100 mg/kg ACT group ($p < 0.01$).

3.9. Effects of ACT on ROS and SOD in skeletal muscle

Given that excessive oxidative stress can lead to fatigue, we investigated the effects of ACT on oxidative stress in PTX-induced CRF in mice. The results showed that ACT (50, 100 mg/kg) significantly decreased ROS levels in mice compared to the PTX group ($p < 0.05$) (Fig. 4C, F). Moreover, ACT (50, 100 mg/kg) also increased SOD activity in mice compared to the PTX group ($p < 0.01$) (Fig. 4G). These findings suggest that the anti-fatigue effect of ACT could be attributed to a certain extent to its anti-oxidative properties.

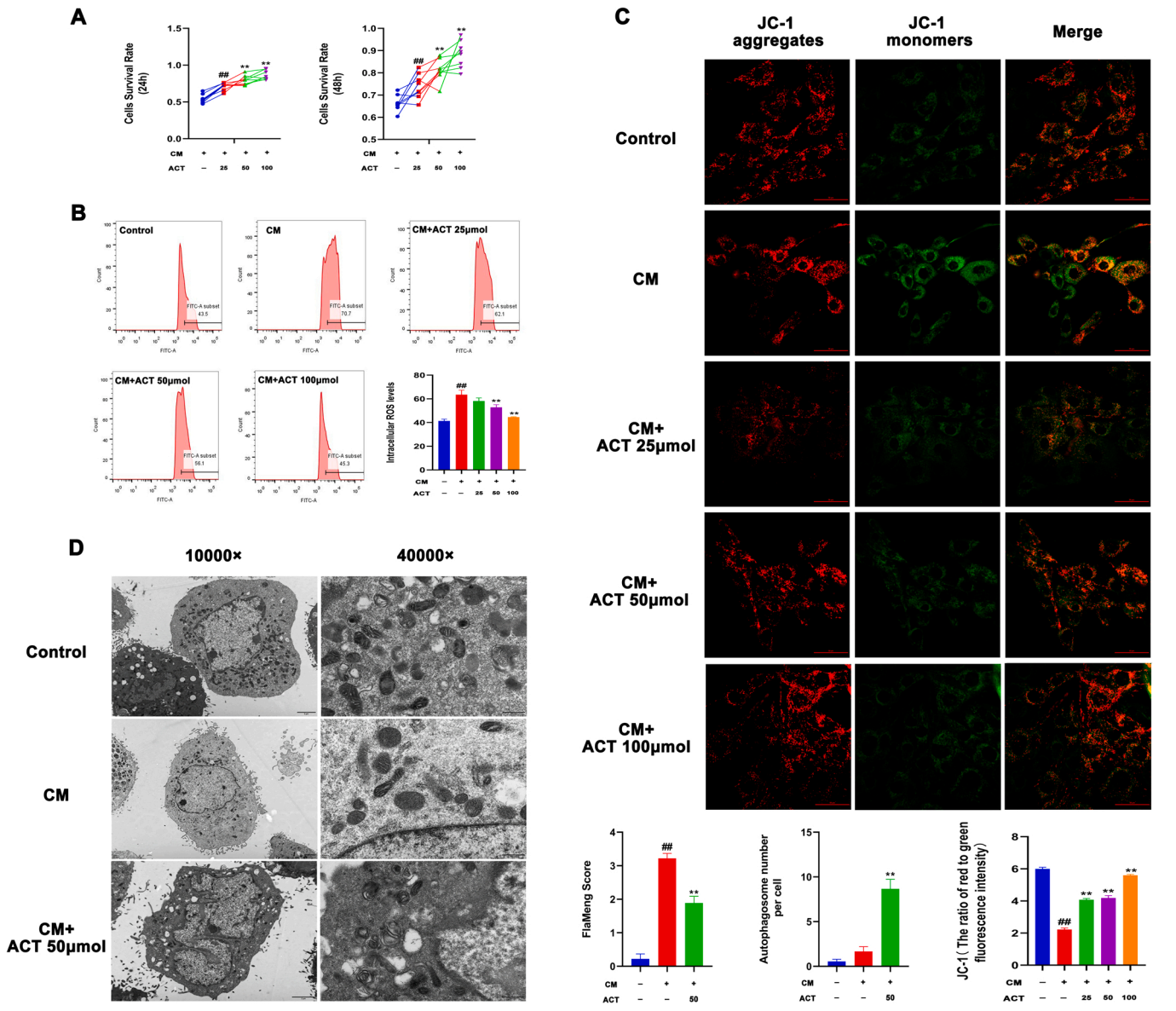

Fig. 5. Mitophagy in C2C12 cells. C2C12 cells were treated with a 33% C26 conditioned medium for 24 h with different concentrations of ACT (25, 50 and 100 μM). A, the cell viability was assessed by CCK-8 assays; B, the level of intracellular ROS was detected by Flow cytometry; C, mitochondrial membrane potential was detected by JC-1 probe, when the mitochondrial membrane potential is high, JC-1 aggregated in the mitochondrial matrix to form J-aggregates, which produce red fluorescence; when the mitochondrial membrane potential is low, JC-1 could not gather in the mitochondrial matrix, and JC-1 is a monomer, producing green fluorescence.; D, representative images of the mitochondrial ultrastructure in C2C12 cells under transmission electron microscopy (scale bar =2 μm and 500 nm). The values are presented as mean ± SD of three independent experiments. #P < 0.05, ##P < 0.01, compared with control group, *P < 0.05, **P < 0.01, compared with model group.

3.10. Transmission electron microscope changes of the effect of ACT on the skeletal muscle ultrastructure

Under transmission electron microscopy, the skeletal muscle structure of the PTX group was seriously damaged compared to the control group. The structure of skeletal muscle mitochondria was swollen, with an irregular shape. The membrane was dissolved and connected, and the internal crest was disordered($p < 0.01$). However, after ACT(100 mg/kg) treatment, the morphology of mitochondria in the PTX group was intact and regularly arranged, but mild swelling could be observed ($p < 0.01$) (Fig. 4D).

3.11. Cell proliferation in C2C12 cells cultured with 33% C26 conditioned medium and ACT

To establish a cachexia model of muscle cell carcinoma in C2C12 cells, a 33% C26 conditioned medium was used as an inducer. CCK-8 assays were performed to determine the effective concentration of C26 conditioned medium and ACT in C2C12 cells. As indicated by Fig. 5A, a dose of 33% C26 conditioned medium and 25, 50, and 100 μM ACT were chosen for the subsequent studies. In addition, we found that the 33% C26 conditioned medium induced a decrease in viability of C2C12 cells, and this phenomenon was reversed after treatment with 25, 50, and 100 μM ACT at 24 h and 48 h ($p < 0.01$).

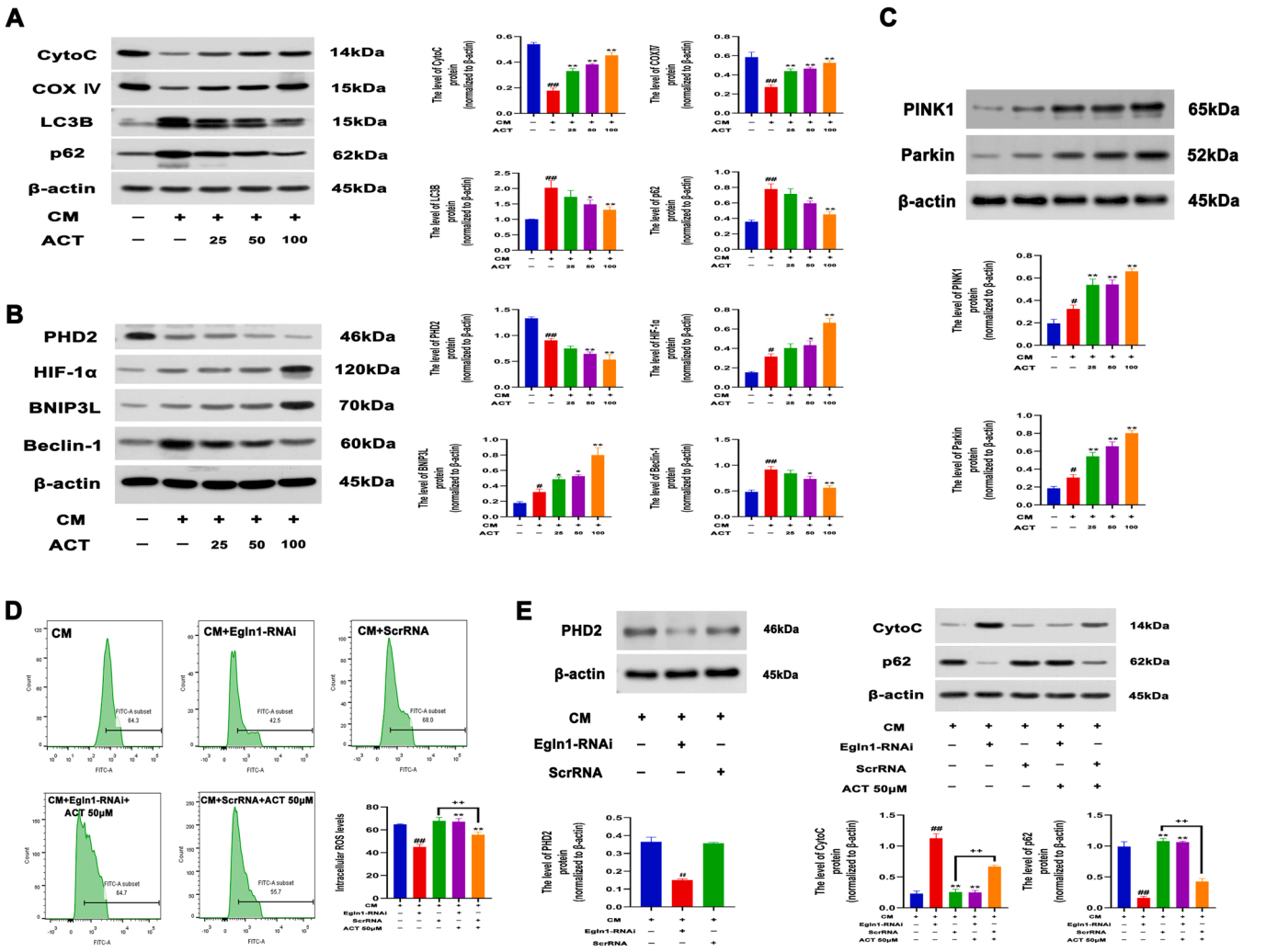

Fig. 6. ACT regulated the HIF-1α/BNIP3 signaling pathway via inhibition of PHD2 expression. C2C12 cells were treated with a 33% C26 conditioned medium for 24 h with different concentrations of ACT (25, 50 and 100 μM). Western blot was used to quantify protein expression levels. Flow cytometry was used to detect the level of intracellular ROS in each group. A-C, the protein expression levels of CytoC, COX IV, LC3B, p62, PHD2, HIF-1α, BNIP3, Beclin-1 PINK1 and Parkin in C2C12 cells. #P < 0.05, ##P < 0.01, compared with control group, *P < 0.05, **P < 0.01, compared with model group; D, the level of intracellular ROS with Egln1-RNAi plasmid in C2C12 cells; E, the protein expression levels of PHD2, CytoC and COX IV in C2C12 cells. β-actin served as a loading control. #P < 0.05, ##P < 0.01, compared with C26 conditioned medium group, *P < 0.05, **P < 0.01, compared with C26 conditioned medium +Egln1-RNAi group, +P < 0.05, ++P < 0.01, compared with C26 conditioned medium + ScrRNA group.

3.12. Effect of ACT on ROS accumulation in C2C12 cells induced by 33% C26 conditioned medium

To identify the protective mechanisms of ACT in C26 conditioned medium-treated C2C12 cells, we assessed whether ACT could alleviate the C2C12 cell response to oxidative stress. In addition, we quantified the intracellular ROS levels. The results showed that stimulation with 33% C26 conditioned medium significantly increased intracellular ROS production ($p < 0.01$), whereas treatment with ACT (50, 100 μM) could effectively decrease the generation of ROS ($p < 0.01$) (Fig. 5B).

3.13. Effects of ACT on the Mitochondrial membrane potential of C2C12 cells cultured in 33% C26 conditioned medium

To investigate whether ACT leads to mitochondrial changes in C2C12 cells, we measured the mitochondrial membrane potential by JC-1 probe. As shown in Fig. 5C, a significant decrease in red fluorescence intensity and an increase in green fluorescence intensity were observed in C26 conditioned medium-treated C2C12 cells ($p < 0.01$). However, administration of ACT (25, 50, and 100 μM) significantly increased red fluorescence intensity and decreased green fluorescence intensity ($p < 0.01$).

3.14. Effects of ACT on the ultrastructure and mitochondrial autophagosomes of C2C12 cells cultured in 33% C26 conditioned medium

As demonstrated in Fig. 5D, stimulation with the C26 conditioned medium for 24 h resulted in a significant increase in the percentage of cells with fragmented mitochondria compared with the control ($p < 0.01$). Treatment with 50 μM ACT significantly decreased the percentage of fragmented mitochondria and increased the number of autophagosomes in C26 conditioned medium-treated C2C12 cells ($p < 0.01$).

3.15. Effect of ACT on the protein expressions of autophagy, mitochondrial function and HIF-1 pathway in C2C12 cells induced by 33% C26 conditioned medium

The morphology of mitochondria is closely related to their function. The protein expression levels of COXIV, CytoC, LC3B, p62, PINK1 and

Parkin, which reflect the key functional indexes of mitochondria, were assessed in the control group, C26 conditioned medium group and C26 conditioned medium + different final concentrations (25, 50, 100 μM) ACT group, with β-actin as the internal reference. We found that the expression of COX IV and CytoC in the C26 conditioned medium group was significantly lower than in the control group($p < 0.01$). In contrast, the expression of LC3B and p62 was significantly higher in the C26 conditioned medium group ($p < 0.01$). Compared with the C26 conditioned medium group, the expression of COX IV and CytoC in the C26 conditioned medium + different final concentrations (25, 50, and 100 μM) ACT group increased significantly($p < 0.01$), while the expression of LC3B and p62 decreased significantly. Moreover, ACT (25, 50, and 100 μM) significantly increased PINK1 and Parkin compared to the C26 conditioned medium group ($p < 0.01$). Furthermore, the PHD2/HIF-1α/BNIP3 pathway was analyzed. The results showed that compared with the C26 conditioned medium group, the expression of PHD2 protein decreased significantly, while the expression of HIF-1α, BNIP3 and Beclin-1 increased significantly (Fig. 6A-C).

3.16. Effect of ACT on ROS and the protein expressions of mitochondrial function in C2C12 cells induced by 33% C26 conditioned medium with Egln1-RNAi plasmid

We established that ACT could decrease the expression levels of PHD2 protein and increase the expression of its downstream targets. Next, we sought to explore whether inhibition of PHD2 could suppress the effects of ACT on mitophagy by Egln1-RNAi, a specific PHD2 knockdown plasmid (Fig. 6D-E). Compared with the C26 conditioned medium group, the intracellular ROS content, p62 and PHD2 protein expression decreased significantly, and CytoC protein expression increased significantly in the C26 conditioned medium + Egln1-RNAi group's ($p < 0.01$). In contrast, the intracellular ROS content, p62, CytoC and PHD2 protein expression in the C26 conditioned medium + ScrRNA group did not change significantly ($p > 0.05$). Compared with the C26 conditioned medium + Egln1-RNAi group, the intracellular ROS content, p62 protein expression increased significantly, and CytoC protein expression decreased significantly in C26 conditioned medium + ScrRNA group and C26 conditioned medium + Egln1-RNAi + ACT group ($p < 0.01$). Moreover, compared with the C26 conditioned medium + ScrRNA group, the intracellular ROS content and p62 protein expression were significantly decreased, and the CytoC protein expression was significantly increased in the C26 conditioned medium + ScrRNA + ACT group ($p < 0.01$). The above results indicate that ACT affects intracellular ROS levels, mitochondrial function and mitophagy by mediating PHD2 expression levels.

4. Discussion

It is widely acknowledged that malignant tumors can spread to healthy tissues in other parts of the body and are difficult to treat, becoming a serious public health concern. During tumor occurrence, development, treatment, and rehabilitation, cancer patients often feel very tired and complain of a lack of strength, which does not improve after resting. Accordingly, the academic circle has put forward the concept of cancer-related fatigue, which has gradually become a topic of concern in the field of oncology [17]. It has been established that the occurrence of CRF is related to cancer or the treatment of cancer, interferes with the normal life of patients, significantly affects the quality of life and the treatment of cancer patients. Hence, it is necessary to explore the pathogenesis and develop novel therapeutic measures [18].

The etiology of CRF is complex, encompassing both peripheral and central mechanisms, which have been hypothesized to contribute to overall fatigue in cancer patients. Generally, CRF is mainly induced by energy metabolism disruption in skeletal muscles and neuroinflammation in the CNS [19]. The skeletal muscle is a high metabolic organ that needs adequate ATP generation. The mitochondrial content in skeletal muscle tissue is rich and is the main place of energy conversion and biological oxidation, termed the "energy factory" of cells [20]. Research has shown that chemotherapy nonspecifically targets the skeletal musculature, especially the mitochondria, inducing adverse side effects such as mitochondrial dysfunction due to low energy supply and high oxidative stress [21]. During oxidative phosphorylation, mitochondria produce ROS and other by-products, which cause oxidative stress; excessive accumulation of ROS leads to further damage to the structure and function of mitochondria [22,23]. Moreover, hypoxia is a common phenomenon in solid tumors. It has been shown that hypoxic stress causes the accumulation and activation of HIF-1α. Activated HIF-1α can regulate the expression of a variety of hypoxia response genes by combining with the corresponding target gene sequences and activating mitophagy to clear damaged mitochondria, to maintain oxygen homeostasis and energy metabolism balance [24]. PHD2 is a key enzyme that regulates the stability of HIF-1α. Interestingly, many potential drugs that improve the function of HIF by inhibiting PHD2 have gone far in clinical trials, and a series of recent studies have proved their clinical efficacy in the treatment of anemia. Therefore, the quest for safe and effective PHD2 inhibitors to improve HIF function and increase mitophagy is essential for treating CRF [25].

Cistanche tubulosa is a genus of Orobanchaceae Cistanche, a perennial parasitic herb that is a potent tonic and has a long history as a medicinal plant in China. Modern pharmacological studies have shown that *Cistanche tubulosa* has many properties, such as immune regulation [26], anti-fatigue [27,28], anti-oxidative stress [29], nourishing liver and kidney [30,31]. In our study, molecular docking virtual screening was used to identify potential active components of *Cistanche tubulosa* similar to PHD2 inhibitors. ACT exhibited the highest docking score (−11.184), suggesting it has a good binding affinity with PHD2 protein. Then we used SPR technology to verify the docking results in vitro. To explore the potential mechanism of ACT against CRF, we carried out animal experiments and cell experiments in vivo.

Disease models involve using model organisms to study the pathogenesis of diseases. Clinically, tumor patients undergo radiotherapy to kill tumor cells; however, radiation can also cause damage to the functions of normal body cells. A CRF model induced by radiation was used to simulate clinical practice to observe the fatigue state of mice [32,33]. Moreover, a CRF model of tumor-bearing mice in the late stage of cachexia was established. The tumor-bearing mice were subcutaneously inoculated with tumor cells or tumor cells inoculated into the corresponding organs to replicate the carcinoma model in situ. The fatigued state of mice was observed in the late time window of the natural survival state of tumor mice [34,35]. Moreover, a CRF model induced by chemotherapeutic drugs was based on the drug properties of the chemotherapeutic drugs used by tumor patients, which inevitably damaged normal cell function and induced a sense of fatigue in patients. This model was established to mimic clinical chemotherapy [36,37]. The chemotherapeutic drug PTX used in this experiment was a new anti-microtubule drug, which exerts its effect by maintaining the stability of tubulin and inhibiting cell mitosis via promoting tubulin polymerization and inhibiting its depolymerization. However, the adverse reactions of PTX are relatively large, including allergic reactions, neurotoxicity, myelosuppression, cardiovascular toxicity, gastrointestinal reactions, muscle and joint pain, hepatotoxicity, hair loss and local reactions, etc. Importantly, the incidence and severity of adverse reactions are dose-dependent. Moreover, the adverse reactions of PTX, especially neurotoxicity and muscle and joint pain, are also important causes of chemotherapy-related fatigue [38]. Accordingly, PTX (10 mg/kg, iv for 5 days) has been used to establish an animal model of chemotherapy-related fatigue [36].

In this study, there was no significant difference in mental state, activity, diet and fur appearance among each group of mice at baseline. The mice in each group were lively and active; their fur was smooth and neat. They exhibited sensitivity to food and could quickly escape. There was no significant change in the above observations in the control group

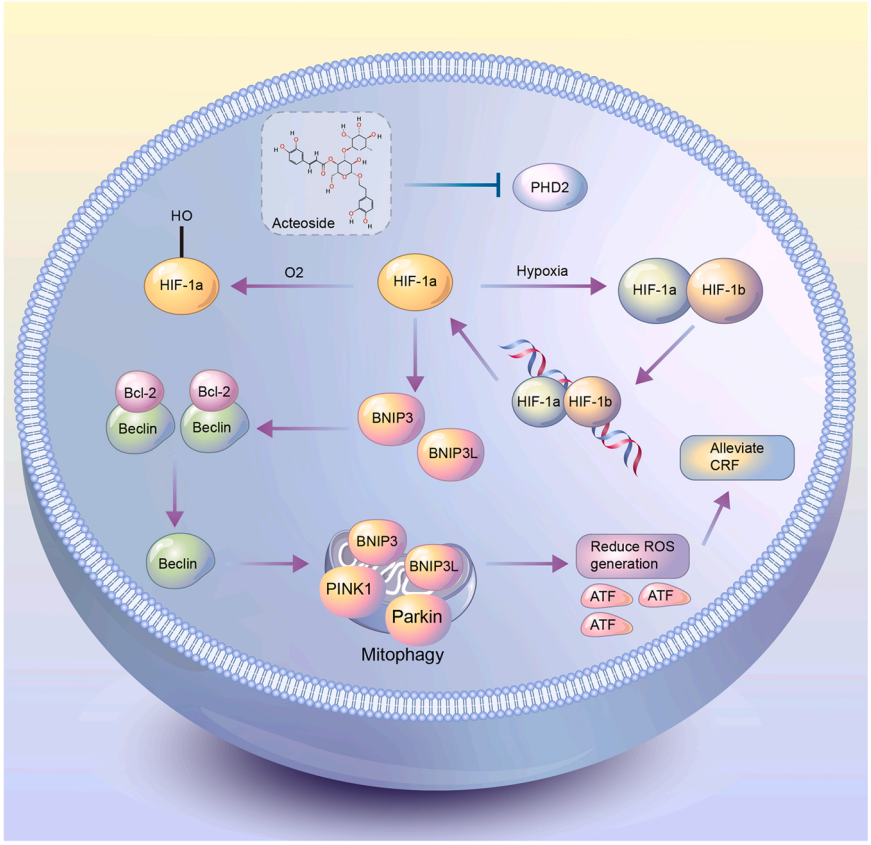

Fig. 7. The putative mechanistic diagram of the enhancing effect of ACT on mitophagy via suppression of PHD2 expression.

during the whole experiment. Compared with the control group, mice in the other groups gradually exhibited sparse hair, aggregation, inactivation, retardation and reduced food intake. Overall, the general condition of mice in the PTX + ACT group was better than in the PTX model group. The above results suggest that ACT administration could improve the mental state, activity, diet and fur appearance of PTX to some extent. Moreover, the exhaustive swimming test showed that ACT could significantly alleviate the decline of swimming ability of mice induced by PTX. Similar results were observed in the open field test and tail suspension test. To sum up, we provided compelling evidence that ACT can significantly improve fatigue induced by PTX. Then, to explore the relationship between CRF and skeletal muscle mitophagy and the mechanism of ACT, we analyzed the skeletal muscle content of each group of mice. Micro-CT showed that the muscle mass of the PTX model mice was decreased, and HE staining further confirmed the phenomenon of muscle atrophy in PTX model mice. Muscle fiber staining showed few slow-twitch muscle fibers in the PTX group. Importantly, treatment with ACT could significantly alleviate the above changes. It has been reported that after treatment with chemotherapy or radiotherapy, the normal structure and function of skeletal muscle mitochondria are damaged involving different signaling pathways, and the structure of the mitochondrial membrane is irregularly arranged. Besides, slow-twitch muscle fibers of skeletal muscle are rich in mitochondria and high in myoglobin content. These results are consistent with our experimental results; PTX-induced damage can be reversed to some extent by treatment with 100 mg/kg of ACT.

According to the literature, mitophagy is maintained at a low level under normal conditions, activated under ischemia, hypoxia and hunger, and degrades by wrapping the damaged mitochondria to lysosomes [39]. Therefore, mitophagy is an important endogenous protective mechanism. It has been shown that autophagy is very important for the clearance of dysfunctional mitochondria in skeletal muscle. The disruption of this process can lead to the rapid accumulation of dysfunctional mitochondria and a decline in muscle mass. The present study found that the C26 conditioned medium could significantly reduce cell survival rate, destroy mitochondria, and induce autophagosome aggregation. These findings may be attributed to a series of cytokines secreted by C26 cells, including IL-6, TNF-α, IL-1β, IFN-γ and leukemia inhibitory factors that play an important role in disrupting energy metabolism in skeletal muscle cells. Our results suggest that the C26 conditioned medium could induce mitophagy but not the timely clearance of damaged mitochondria. Recent studies indicated that autophagy has a complex and close relationship with hypoxia. Evidence from various mammalian cell types indicates that HIF-1α induces autophagy by activating BNIP3, and the enhanced stability of HIF-1α is closely related to a decrease in PHD2 activity [40]. It has been established that autophagy involves the formation of autophagosomes, and this mechanism is initiated by the dissociation of the Beclin1/Bcl-2 complex. HIF-1 mediates the increase in BNIP3 expression during skeletal muscle exposure to hypoxia. Importantly, BNIP3 can compete with Beclin1 for binding to Bcl-2, leading to the release of Beclin1, thus promoting the initiation of autophagy and mitophagy [41].

In the early stages of our study, we conducted KEGG pathway enrichment of the common targets of *Cistanche tubulosa* and CRF using network pharmacology. The results showed that the HIF-1 signaling pathway was ranked second among the top 20 related pathways. These results were verified in the mouse cancer cachexia model induced by H22 hepatoma cells. Nonetheless, the specific regulatory mechanism of *Cistanche tubulosa* in cancer-related fatigue mediated by HIF-1 α remains largely unknown. This study confirmed that ACT, the landmark component of *Cistanche tubulosa*, could promote mitophagy with accelerated clearance of autophagosomes, thus increasing cell viability, reducing intracellular ROS levels and increasing mitochondrial membrane potential. In addition, this study further confirmed that the PHD2/

HIF-1α/BNIP3 pathway is an important signaling hub in ACT-enhancing mitophagy. The expression levels of autophagy-associated proteins, mitochondrial functional proteins and HIF-1 signaling pathway proteins were quantified by Western-blot. We found that ACT could significantly upregulate the expression levels of mitochondrial functional proteins COXIV, CytoC, HIF-1α, BNIP3, PINK1 and Parkin, and significantly downregulate the expression of autophagy marker proteins p62, LC3B PHD2, and Beclin-1. We found that the protective effect of ACT disappeared when a PHD2 gene knockdown plasmid Egln-1-RNAi was used, suggesting that PHD2 is a key target protein involved in regulating mitophagy, and ACT promotes mitophagy against CRF through the PHD2/HIF-1α/BNIP3 signaling pathway.

5. Conclusion

The present work demonstrated that ACT could promote mitophagy by suppressing PHD2 expression to remove dysfunctional mitochondria and alleviate CRF (Fig. 7). These findings provide novel insights into the mechanisms of this new drug formulation for the future treatment of CRF. However, the underlying mechanisms are more complex than described here, and our results do not exclude the possible involvement of other mechanisms caused by ACT to treat CRF.

Ethics statement

The animal study was reviewed and approved by the Experimental Animal Ethics Committee of Xinjiang Medical University (1ACUC-20210309-06).

Author contributions

Tao Liu: Conceptualization. **Jian-hua Yang:** Conceptualization, Writing – review & editing, Supervision. **Jun-ping Hu:** Conceptualization, Funding acquisition, Supervision. **Shi-lei Zhang:** Data curation, Writing – original draft. **Fu-kai Gong:** Data curation, Project administration. **Jia-li Liu:** Data curation, Project administration.

Funding

This study was supported by the Key Projects of Natural Science Foundation of Xinjiang Uygur Autonomous Region (2021D01D11), the China Postdoctoral Science Foundation (2021MD703894), the Key Laboratory of Active Components of Xinjiang Natural Medicine and Drug Release Technology (No. XJDX1713), and the National Natural Science Foundation of China (No. 81860735).

Data Availability

The raw data supporting the conclusions of this article will be made available by the authors, without undue reservation, to any qualified researcher.

Acknowledgments

The authors thank the whole team for assistance.

Appendix A. Supporting information

Supplementary data associated with this article can be found in the online version at doi:10.1016/j.biopha.2022.113004.

References

[1] A.M. Berger, K. Mooney, A. Alvarez-Perez, W.S. Breitbart, K.M. Carpenter, D. Cella, C. Cleeland, E. Dotan, M.A. Eisenberger, C.P. Escalante, P.B. Jacobsen, C. Jankowski, T. LeBlanc, J.A. Ligibel, E.T. Loggers, B. Mandrell, B.A. Murphy, O. Palesh, W.F. Pirl, S.C. Plaxe, M.B. Riba, H.S. Rugo, C. Salvador, L.I. Wagner, N. D. Wagner-Johnston, F.J. Zachariah, M.A. Bergman, C. Smith, Cancer-related fatigue, version 2.2015, J. Natl. Compr. Cancer Netw. 13 (2015) 1012–1039.
[2] J.E. Bower, Cancer-related fatigue-mechanisms, risk factors, and treatments, Nat. Rev. Clin. Oncol. 11 (2014) 597–609.
[3] F. Cramp, J. Byron-Daniel, Exercise for the management of cancer-related fatigue in adults, Cochrane Database Syst. Rev. (2012).
[4] S. Yang, S. Chu, Y. Gao, Q. Ai, Y. Liu, X. Li, N. Chen, A NArrative Review of Cancer-related Fatigue (CRF) and its possible pathogenesis, Cells 8 (2019).
[5] J.M. Argiles, F.J. Lopez-Soriano, S. Busquets, Muscle wasting in cancer: the role of mitochondria, Curr. Opin. Clin. Nutr. Metab. Care 18 (2015) 221–225.
[6] X. Wang, J. Mao, T. Zhou, X. Chen, H. Tu, J. Ma, Y. Li, Y. Ding, Y. Yang, H. Wu, X. Tang, Hypoxia-induced myeloid derived growth factor promotes hepatocellular carcinoma progression through remodeling tumor microenvironment, Theranostics 11 (2021) 209–221.
[7] D.T. Dave, B.M. Patel, Mitochondrial metabolism in cancer cachexia: novel drug target, Curr. Drug Metab. 20 (2019) 1141–1153.
[8] G. Favaro, V. Romanello, T. Varanita, M.A. Desbats, V. Morbidoni, C. Tezze, M. Albiero, M. Canato, G. Gherardi, D. De Stefani, C. Mammucari, B. Blaauw, S. Boncompagni, F. Protasi, C. Reggiani, L. Scorrano, L. Salviati, M. Sandri, DRP1-mediated mitochondrial shape controls calcium homeostasis and muscle mass, Nat. Commun. 10 (2019).
[9] H.-M. Ni, J.A. Williams, W.-X. Ding, Mitochondrial dynamics and mitochondrial quality control, Redox Biol. 4 (2015) 6–13.
[10] K. Palikaras, E. Lionaki, N. Tavernarakis, Mechanisms of mitophagy in cellular homeostasis, physiology and pathology, Nat. Cell Biol. 20 (2018) 1013–1022.
[11] S.Y. Oh, J.Y. Seok, Y.S. Choi, S.H. Lee, J.-S. Bae, Y.M. Lee, The histone methyltransferase inhibitor BIX01294 inhibits HIF-1 alpha stability and angiogenesis, Mol. Cells 38 (2015) 528–534.
[12] Y.-L. He, L.-Y. Wu, L.-L. Zhu, M. Fan, The role of mitophagy in hypoxic adaptation, Prog. Biochem. Biophys. 39 (2012) 217–223.
[13] Y. Wu, N. Wang, Y. Lei, T. Hu, Q. You, X. Zhang, Small-molecule inhibitors of HIF-PHD2: a valid strategy to renal anemia treatment in clinical therapy, Medchemcomm 7 (2016) 1271–1284.
[14] Y. Wu, Z. Jiang, Q. You, X. Zhang, Application of in-vitro screening methods on hypoxia inducible factor prolyl hydroxylase inhibitors, Bioorg. Med. Chem. 25 (2017) 3891–3899.
[15] T.F. Najafi, N. Bahri, H.R. Tohidinik, S. Feyz, F. Bloki, S. Savarkar, S. Jahanfar, Treatment of cancer-related fatigue with ginseng: a systematic review and meta-analysis, J. Herb. Med. 28 (2021).
[16] L.-l Wang, H. Ding, H.-s Yu, L.-F. Han, Q.-h Lai, L.-j Zhang, X.-b Song, Cistanches herba: chemical constituents and pharmacological effects, Chin. Herb. Med. 7 (2015) 135–142.
[17] K.M. Mustian, C.M. Alfano, C. Heckler, A.S. Kleckner, I.R. Kleckner, C.R. Leach, D. Mohr, O.G. Palesh, L.J. Peppone, B.F. Piper, J. Scarpato, T. Smith, L.K. Sprod, S. M. Miller, Comparison of pharmaceutical, psychological, and exercise treatments for cancer-related fatigue a meta-analysis, Jama Oncol. 3 (2017) 961–968.
[18] Y. Ma, B. He, M. Jiang, Y. Yang, C. Wang, C. Huang, L. Han, Prevalence and risk factors of cancer-related fatigue: a systematic review and meta-analysis, Int. J. Nurs. Stud. 111 (2020).
[19] M. Mashimo, J. Moss, Functional role of ADP-Ribosyl-acceptor hydrolase 3 in poly (ADP-Ribose) polymerase-1 response to oxidative stress, Curr. Protein Pept. Sci. 17 (2016) 633–640.
[20] A. Diaz-Vegasa, V. Eisner, E. Jaimovich, Skeletal muscle excitation-metabolism coupling, Arch. Biochem. Biophys. 664 (2019) 89–94.
[21] J.A. Carson, J.P. Hardee, B.N. VanderVeen, The emerging role of skeletal muscle oxidative metabolism as a biological target and cellular regulator of cancer-induced muscle wasting, Semin. Cell Dev. Biol. 54 (2016) 53–67.
[22] D.B. Zorov, M. Juhaszova, S.J. Sollott, Mitochondrial reactive oxygen species (ROS) and ros-induced ros release, Physiol. Rev. 94 (2014) 909–950.
[23] P. Fan, X.-H. Xie, C.-H. Chen, X. Peng, P. Zhang, C. Yang, Y.-T. Wang, Molecular regulation mechanisms and interactions between reactive oxygen species and mitophagy, DNA Cell Biol. 38 (2019) 10–22.
[24] F.B. Favier, F.A. Britto, D.G. Freyssenet, X.A. Bigard, H. Benoit, HIF-1-driven skeletal muscle adaptations to chronic hypoxia: molecular insights into muscle physiology, Cell. Mol. Life Sci. 72 (2015) 4681–4696.
[25] I. Daskalaki, I. Gkikas, N. Tavernarakis, Hypoxia and selective autophagy in cancer development and therapy, Front. Cell Dev. Biol. 6 (2018).
[26] S.-P. You, J. Zhao, L. Ma, M. Tudimat, S.-L. Zhang, T. Liu, Preventive effects of phenylethanol glycosides from Cistanche tubulosa on bovine serum albumin-induced hepatic fibrosis in rats, Daru-J. Pharm. Sci. 23 (2015).
[27] T. Wang, X. Zhang, W. Xie, Cistanche deserticola Y. C. Ma, “desert ginseng”: a review, Am. J. Chin. Med. 40 (2012) 1123–1141.
[28] M. Li, X. Tian, X. Li, T. Mao, T. Liu, Anti-fatigue activity of gardenia yellow pigment and Cistanche phenylethanol glycosides mixture in hypoxia. Food, Bioscience 40 (2021).
[29] M. Deng, J.Y. Zhao, X.D. Ju, P.F. Tu, Y. Jiang, Z.B. Li, Protective effect of tubuloside B on TNF alpha-induced apoptosis in neuronal cells, Acta Pharmacol. Sin. 25 (2004) 1276–1284.
[30] W.-T. Xiong, L. Gu, C. Wang, H.-X. Sun, X. Liu, Anti-hyperglycemic and hypolipidemic effects of Cistanche tubulosa in type 2 diabetic db/db mice, J. Ethnopharmacol. 150 (2013) 935–945.
[31] S.-L. Zhang, L. Ma, J. Zhao, S.-P. You, X.-T. Ma, X.-Y. Ye, T. Liu, The phenylethanol glycoside liposome inhibits PDGF-induced HSC activation via regulation of the FAK/PI3K/Akt signaling pathway, Molecules 24 (2019).

[32] M. Renner, R. Feng, D. Springer, M.-K. Chen, A. Ntamack, A. Espina, L.N. Saligan, A murine model of peripheral irradiation-induced fatigue, Behav. Brain Res. 307 (2016) 218–226.
[33] B.S. Wolff, M.A. Renner, D.A. Springer, L.N. Saligan, A mouse model of fatigue induced by peripheral irradiation, Jove-J. Vis. Exp. (2017).
[34] D.M. Norden, R. Devine, S. Bicer, R. Jing, P.J. Reiser, L.E. Wold, J.P. Godbout, D. O. McCarthy, Fluoxetine prevents the development of depressive-like behavior in a mouse model of cancer related fatigue, Physiol. Behav. 140 (2015) 230–235.
[35] D.M. Norden, S. Bicer, Y. Clark, R. Jing, C.J. Henry, L.E. Wold, P.J. Reiser, J. P. Godbout, D.O. McCarthy, Tumor growth increases neuroinflammation, fatigue and depressive-like behavior prior to alterations in muscle function, Brain Behav. Immun. 43 (2015) 76–85.
[36] M.A. Ray, R.A. Trammell, S. Verhulst, S. Ran, L.A. Toth, Development of a mouse model for assessing fatigue during chemotherapy, Comp. Med. 61 (2011) 119–130.
[37] J.P. Dougherty, B.S. Wolff, M.J. Cullen, L.N. Saligan, M.C. Gershengorn, Taltirelin alleviates fatigue-like behavior in mouse models of cancer-related fatigue, Pharmacol. Res. 124 (2017) 1–8.
[38] M. Naganuma, K. Tahara, S. Hasegawa, A. Fukuda, S. Sasaoka, H. Hatahira, Y. Motooka, S. Nakao, R. Mukai, K. Hirade, T. Yoshimura, T. Kato, H. Takeuchi, M. Nakamura, Adverse event profiles of solvent-based and nanoparticle albumin-bound paclitaxel formulations using the food and drug administration adverse event reporting system, Sage Open Med. 7 (2019).
[39] S.-M. Yoo, Y.-K. Jung, A molecular approach to mitophagy and mitochondrial dynamics, Mol. Cells 41 (2018) 18–26.
[40] L. Singh, S. Aldosary, A.S. Saeedan, M.N. Ansari, G. Kaithwas, Prolyl hydroxylase 2: a promising target to inhibit hypoxia-induced cellular metabolism in cancer cells, Drug Discov. Today 23 (2018) 1873–1882.
[41] A.H. Chourasia, K.F. Macleod, Tumor suppressor functions of BNIP3 and mitophagy, Autophagy 11 (2015) 1937–1938.